



Originally published as:

Moeck, I., Schandelmeier, H., Holl, H.-G. (2009): The stress regime in a Rotliegend reservoir of the Northeast German Basin. - International Journal of Earth Sciences, 98, 7, 1643-1657

DOI: 10.1007/s00531-008-0316-1

The stress regime in a Rotliegend reservoir of the Northeast German Basin

Inga Moeck, Heinz Schandelmeier, Heinz-Gerd Holl

*I. Moeck, H.-G. Holl**

GFZ Potsdam, Section Geothermics, Telegrafenberg, D-14473 Potsdam, Germany

E-mail: moeck@gfz-potsdam.de

Tel.: +49-331-2881573

Fax: +49-331-2881577

H. Schandelmeier

TU Berlin, Institut für Angewandte Geowissenschaften, Ernst-Reuter-Platz 1, D-10587 Berlin, Germany

**now at: Schlumberger Oilfield Australia Pty Ltd., 127 Creek Street, Brisbane, QLD 4000, Australia*

Abstract In-situ stresses have significant impact, either positive or negative, on the short and long term behaviour of fractured reservoirs. The knowledge of the stress conditions are therefore important for planning and utilization of man-made geothermal reservoirs. The geothermal field Groß Schönebeck (40 km north of Berlin/Germany) belongs to the key sites in the northeastern German Basin. We present a stress state determination for this Lower Permian (Rotliegend) reservoir by an integrated approach of 3D structural modelling, 3D fault mapping, stress ratio definition based on frictional constraints, and slip-tendency analysis. The results indicate stress ratios of the minimum horizontal stress S_{hmin} being equal or increasing 0.55 times the amount of the vertical stress S_V ($S_{hmin} \geq 0.55 \cdot S_V$) and of the maximum horizontal stress $S_{Hmax} \leq 0.78-1.00 \cdot S_V$ in stress regimes from normal to strike slip faulting. Thus, acting stresses in the 4,100 m deep reservoir are $S_V=100$ MPa, $S_{hmin} = 55$ MPa and $S_{Hmax} = 78 -100$ MPa. Values from hydraulic fracturing support these results. Various fault sets of the reservoir are characterized in terms of their potential to conduct geothermal fluids based on their slip and dilatation tendency. This combined approach can be adopted to any other geothermal site investigation.

Keywords *North East German Basin, Rotliegend fault pattern, 3D geological modelling, recent stress field, frictional equilibrium, slip-tendency analysis*

Abbreviations

NEGB North East German Basin, S_{Hmax} : maximum horizontal stress, S_{hmin} : minimum horizontal stress, S_V : vertical stress, S_1 : maximum principle stress, S_2 : intermediate principle stress, S_3 : minimum principle stress

Introduction

The North East German Basin (in the following abbreviated as NEGB) is part of the North German Basin, that extends from the dutch-german to the german-polish border. The present day structure of the NEGB is well constrained in lithospheric scale by continuous reflections down to the base of Upper Permian (Zechstein) (Marotta et al. 2000). Also the complex polyphase history of the basin from Carboniferous to Cenozoic is inferred e. g. from the DEKORP seismic line (Scheck et al. 1999; Scheck and Bayer 1999). Thermomechanical models describe primarily the lithospheric structure and the two distinct strength boundaries in the seismic Moho and the Zechstein salt level (Marotta et al. 2000) rather than a fault pattern at a scale that is adequate for exploration.

For a geothermal site investigation a detailed 3D geological model is needed to understand the subsurface structure with focus on fault pattern and sedimentary record of Lower Permian (Rotliegend) reservoir rock. In this present study 2D seismic and well data of former gas exploration in East Germany are re-used to develop a 3D model from Quaternary to Carboniferous. There is special interest in the stress field of the reservoir at 4,100 m depth since the in-situ stresses are of fundamental importance for understanding the mechanical behaviour and permeability development in a geothermal reservoir.

The geothermal investigation site Groß Schönebeck (40 km north of Berlin/Germany) belongs to the key sites of geothermal exploration studies in the North German Basin. The geothermal aquifer is part of the Rotliegend siliciclastica of the NEGB, which are ongoing to be explored for planned geothermal energy production. On a larger scale, the NEGB and in particular the geothermal aquifer is located at the transition zone between the South Permian Basin and the Polish Trough (Fig. 1a) and belongs to the eastern periphery of the South Permian Basin (Scheck et al. 2002). At the Groß Schönebeck site a gas exploration well, drilled in 1990 to a depth of approximately 4,300 m and abandoned due to non-productivity, was re-opened by the GFZ Potsdam in 2000 currently being used as geothermal in-situ laboratory (Fig. 1b). Several hydraulic stimulation campaigns have been carried out in this well (Legarth et al. 2005). Now a second well was recently drilled by the GFZ Potsdam to establish a well doublet.

It is known from several authors that the hydraulic conductivity of faults and fractures is – among other factors – governed by the in-situ stress field. Faults with high shear stress are known as hydraulically active (Ito & Zoback 2000; Zhang et al. 2002; Zhang et al. 2007). From other authors it is known, that extensional fractures act as fluid-conducting fractures (e.g. Gudmundsson 2000; Gudmundsson et al. 2002). Thus, the discrimination of critically stressed and extensional faults within the current stress field means a first assessment of the hydraulic conductivity of observed or suspected faults in the geothermal aquifer. The present study aims at a detailed description of a newly developed 3D structural model and at the analysis of fault behaviour within the in-situ stress field in the explored geothermal reservoir at 4,100 m depth. A combined approach of 3D fault mapping, in-situ stress regime calculation based on the frictional failure theory (Peška and Zoback 1995 and the references therein) and fault slip-tendency analysis (Morris et al. 1996) is applied to estimate fluid transport in fractured rock. Observations from hydraulic fracturing treatments help to verify the calculated stress field magnitudes (Legarth et al. 2005). The results are particularly important for the planned man-made geothermal reservoir at the site Groß Schönebeck.

Present-day stresses in the North East German Basin

Several authors have analysed the current stress field in the NEGB at a regional scale. Kaiser et al. (2004) presented a finite element-based dynamic modelling study of the recent stress conditions in the NEGB. According to these modelling results, the NEGB experiences recent compressive stress in its northeastern parts, indicating that transpressive or reverse faulting may be the dominant mode of actual deformation. The model results fit to the observation of reactivated basement faults, which are active since Middle Miocene times.

Mazur et al. (2005) also argue that compressive stresses in the mobile Alpine Belt were transmitted along particular crustal zones of weakness into its distant foreland during the Late Cretaceous and Early Tertiary periods. The subsequent inversion in the area of the North German Basin was strongly influenced by the orientation of pre-existing basement structures and by the existence of thick Zechstein salt layers. One of the prominent zones of upper crustal weakness is the

NW-SE oriented Elbe Fault Zone, which bounds the SW of the NEGB at a crustal scale and influenced the basin evolution of the NEGB (Hecht et al. 2003). Thick Zechstein salt layers, however, caused probably decoupling of the stress fields during the inversion period (Scheck et al. 2003; Bayer et al. 2003, Hecht et al. 2003; Röckel and Lempp 2003). The near-surface crust in the NEGB is obviously affected by the far-field stress system generated by the alpine compression front. This is indicated by the fact, that in the subsalinar the directions of the maximum horizontal stress S_{Hmax} form a fanlike shape with a N-S axis whereas in the suprasalinar the directions of S_{Hmax} strongly scatter around E-W directions (Grote 1998; Marotta et al. 2000; Röckel and Lempp 2003; Lempp and Lerche 2006).

Fig. 1

Based on a re-evaluation of hydraulic fracturing and pressure stability test data from numerous drill holes from the eastern part of the NEGB, Röckel and Lempp (2003) have demonstrated that in the subsalinar of the NEGB, the trend of S_{Hmax} is N-S in the central and NNE-SSW in the eastern part of the basin. More importantly the magnitude of the minimum horizontal stress S_{hmin} is, without exception, generally significantly smaller than the magnitude of the vertical stress S_V . Thus, reverse faulting stress regimes might be unlikely in the subsalinar of the NEGB but possibly transitional ($S_{Hmax} = S_V > S_{hmin}$) or strike-slip ($S_{Hmax} > S_V > S_{hmin}$) stress regime conditions may prevail at least locally although there are no indications available that S_{Hmax} exceeds S_V .

The less dense and buoyant salinar sequence shows much more inconsistent stress conditions than the subsalinar. According to Röckel and Lempp (2003), the suprasalinar and subsalinar sequences may be mechanically decoupled, thus not allowing plate tectonic stresses that act in the crust, to be transmitted to the suprasalinar cover sequences. A stress transmission to the mesozoic/cenozoic overburden may however function along large fault systems or where the salinar sequences are missing.

3D model of the Groß Schönebeck site

Development of the 3D geological model

Seismic and well data from the gas exploration in East Germany are re-used for 3D structural modelling. The input data were generated from 1971 to 1990 and comprise six 2D seismic sections and data from 15 deep wells, covering an area of about 1,391 km². The seismic profiles and the base map of profile traces provided as hard copies were digitised, georeferenced and merged into data sets, each file containing the data of one profile. The resolution of the seismic data is lower in the subsalt than in the suprasalt, consequently the reflector of the top Carboniferous is rarely detected. The top of Lower Permian volcanic rock (reflector H6), the top of the Elbe Basis sandstone (reflector R2, formerly called the Eldena 7 cycle) and the top of silt-clay successions in the Hannover formation (reflector R1, formerly called the Base Mellin; the reflectors related to the stratigraphic pile see Fig. 1c) are detected in all seismic sections whereas the Carboniferous is detected in three of the six seismic profiles. The structural description is therefore restricted to the Lower Permian and does not include the Carboniferous fault pattern.

Fault and horizon data are separated in isolated files. The fault model is calculated first because it is the basis for the coherent fault horizon model. The model depth ranges from surface to 5,000 m depth and includes the strata from Quaternary to Carboniferous as picked by the seismic profiles. The input data are interpolated with different interpolation algorithms, depending on the kind of surface that is mapped. A detailed description of the different interpolation algorithms used in the model building process is beyond the scope of this article and is given by Moeck et. al (2006).

Fig. 2

Subsurface structure

The resulting 3D structural model consists of 124 faults and 169 fault blocks, the latter defining the space between the fault planes. The fault pattern is built up of two fault systems decoupled by up to 1,200 m thick Upper Permian (Zechstein)

salt layers (Fig. 2). The dominating Mesozoic structure is an antiform above a 70° trending salt ridge at which the well GrSk 3/90 is located. The salt is moved upwards to a depth of 2,100 m (Fig. 2). In the northwest of the model area, 10 km north of the well GrSk 3/90 a reduced thickness of the salt implies salt movement causing a depression in the suprasalt successions.

The fault system in the suprasalinar is characterised by major faults striking 20°, 100° and 120°, and minor faults oriented in 50° and 160°. The displacement along the faults indicates normal faulting by hanging wall throw down movement.

Oblique strike-slip movement cannot be excluded. Most of the Mesozoic faults are located above salt antiforms and originate in Early to Late Triassic units.

Therefore, many of the Mesozoic faults are interpreted as dilatational faults related to upward salt movement. The depositional record also suggests upward salt movement that was initiated in the Upper Buntsandstein as recorded in the wells of Zehdenick in the northwestern part of the model area.

The structure of the subsalinar is governed by a changing thickness of the volcanic and sedimentary Lower Permian. In Figure 3, eight N-S striking profiles illustrate the structures from Carboniferous to Upper Permian Zechstein salt. The thickness of the Lower Rotliegend volcanic rock varies from zero in the northwestern part to 600 m in the eastern part of the model area. A peak of thick volcanics is situated in the southeastern quadrant of the model area. The Upper Rotliegend siliciclastic sediments show less thickness variations ranging from 400 to 450 m. At some locations, post-Rotliegend faulting is indicated like 10 km north of Groß Schönebeck, where a WNW-ESE trending graben filled with thick volcanic and reduced sedimentary successions evolved on faults that cross-cut the Zechstein base. Eventually, this graben developed in the Upper Permian when the Zechstein basin was formed.

The subsalt fault system consists of 130° striking major faults and 30° and 170° striking minor faults (Fig. 2, and Fig.6C also). A major fault in NE-SW orientation is interpreted with some uncertainty from two seismic sections because the data are very sparse in this model area. The throw along the faults indicates downward movement of the hanging walls by a few meters. This fault system may have been part of the regional wrench fault system, which was active in the post-orogenic period of the variscan orogeny (Ziegler & Dezes 2005). There are no indications of reverse faulting in the modelled area.

Fig. 3

The in situ stress regime in the reservoir

Boundary conditions for frictional equilibrium

Where no information on stress magnitudes is available, it is possible to define the possible stress conditions in any crustal depth assuming that in-situ stress magnitudes in the crust will not exceed the condition for frictional sliding on well-oriented faults (Jaeger et al. 2007; Peška and Zoback 1995). To illustrate the stress conditions for faulted reservoir systems under the wide range of the stress states, some reasonable boundary conditions had to be set to consider the range of possible stress states in the faulted compartment. In extensional regions, principal stresses that are approximately horizontal (S_{Hmax} and S_{Hmin}) may be significantly smaller than the vertical stress (S_V) thus the intermediate and the minimum principle stress directions, S_2 and S_3 respectively, are horizontal and the maximum principle stress direction S_1 is vertical. In contrast, the opposite is true for highly compressional areas (S_1 and S_2 is horizontal, S_3 is vertical) after Andersson's theory of faulting. It is assumed that one of the principal stresses is vertical and that the state of stress within the compartment rocks is in frictional equilibrium. In this case the ratio of effective principal stresses is given by Jaeger et al. (2007) as

$$\frac{(S_1 - P_p)}{(S_3 - P_p)} = \left(\sqrt{\mu^2 + 1} + \mu \right)^2 \quad \text{eq. (1)}$$

where μ , the coefficient of sliding friction, is taken from laboratory measurements to be $0.6 \leq \mu \leq 1.0$ (Byerlee 1978) and P_p is the in-situ pore pressure. Byerlee (1978) has shown in many shear tests on different rock types, that shear failure is defined by a frictional coefficient of $\mu = 0.6$, if the normal stress on the failure plane exceeds 200 MPa, which is equivalent to a crustal depth of 5 to 6 km. At shallower crustal depth from 1 to 5 km normal stresses on fracture planes are generally below the 200 MPa threshold, and a μ -value of 0.85 better defines shear failure. Thus, for the geothermal aquifer of Groß Schönebeck located at 4,100 m depth, a frictional coefficient of $\mu = 0.85$ is assumed. Approximately hydrostatic pore pressure conditions ($P_p = 0.43 * S_V$) are assumed for the aquifer. Equation (1) can be applied in the following way:

$$\frac{(S_1 - P_p)}{(S_3 - P_p)} = \left(\sqrt{0.85^2 + 1} + 0.85 \right)^2$$

$$= 4.68$$

$$S_1 - P_p = 4.68 S_3 - 4.68 P_p$$

$$S_1 + 3.68 P_p = 4.68 S_3 \quad \left| P_p = 0.43 S_v \right.$$

$$S_1 + 1.58 S_v = 4.68 S_3$$

The calculation yields the upper and the lower boundary of any possible stress regimes under the described reservoir conditions of certain depth, pore pressure and friction coefficient:

$$S_{H \max} \leq 3.10 S_v \text{ (for } S_{h \min} = S_v \text{),} \quad \text{eq. (1a)}$$

$$S_{h \min} \geq 0.55 S_v \text{ (for } S_{H \max} = S_v \text{).} \quad \text{eq. (1b)}$$

For higher pore pressures, lower coefficients of friction or stress states that differ from frictional equilibrium, a smaller range of differential stress values may exist. The values of $S_{H \max}$ and $S_{h \min}$ from eq. (1a) and eq. (1b) can be illustrated in a polygonally shaped region (Moos and Zoback 1990 and 1993; Peška and Zoback 1995) that defines the possible stresses by frictional strength of the crust at any depth. The stress states in which the crust is in frictional equilibrium, as given by eq. (1), are marked by points lying at the periphery of the polygon for various tectonic regimes. The stress polygon in Figure 4 represents the potentially stress states and respective stress ratios for the geothermal reservoir rock of 4,100 m deep Lower Permian successions. The state of stress may vary between the highly tensional stress state (radial tension) and the highly compressional stress state (radial compression).

Fig. 4

Estimation of the vertical Stress ($\sigma_{zz} = S_v$)

For a variable density, ρ , with respect to depth, and a gravitational acceleration, $g = 9.81 \text{ m s}^{-2}$, the vertical stress component in a body of rock at depth $z = -D$, follows the relationship

$$\sigma_{zz} = \int_{-D}^0 \rho g dz . \quad \text{eq. (2)}$$

The weight of the overburden is derived from the average weight of major lithostratigraphic unit of the NE German Basin (Table 1 from Kopf 1965) and the thickness of the rock units known from the vertical profile along the well GrSk 3/90. From these weight variations an average density of 2,500 kg*m⁻³ for the entire rock column was calculated. Applying this value to equation (2) we obtain:

$$\sigma_{zz} = S_v = \rho g z = 100 \text{ MPa}, \quad \text{eq. (3)}$$

for $z = 4,100 \text{ m}$.

Taking into account the high salinity of the pore fluid, the pore pressure P_p should be close to hydrostatic with $P_p = 43 \text{ MPa}$ at 4,100 m depth. The effective vertical stress is therefore $S_{\text{veff}} = S_v - P_p = 57 \text{ MPa}$.

In fact, the pore fluid pressure of 43.8 MPa is determined in 4,220 m depth by pressure and slurry rates during fracturing treatments in the geothermal target horizon (Legarth et al. 2005).

Table 1 Lithostratigraphy of the well section GrSk 3/90 and densities for comparable rocks from the NEGB (from Kopf, 1965). The values are used for the calculation of the average density of the overburden rock along the vertical profile of the well GrSk 3/90.

Well GrSk 3/90		Density gradient for NEGB (Kopf, 1965)	
stratigraphy	lithology	depth in meters	Density in kg*m ⁻³
Quaternary	Unconsolidated sand, clay	0 -100	2,100
Tertiary	Sand, clay, marl,	-200	2,200
Cretaceous	marly limestone	-300	2,250
Jurassic		-700	2,350
Upper Triassic	Silt-, clay-, sandstone, gypsum, marl	-1,400	2,550
Middle Triassic	Marly limestone, limestone, anhydrite	like Upper Triassic -3,000	2,650
Lower Triassic	Sand-, silt, claystone,	like Upper Triassic	
Röt-Formation	halite	-3,000	2,180
	anhydrite	-3,000	2,920
	Evaporites:		
	halite		2,180
Upper Permian	gypsum	below -3,000	2,320
	dolomite		2,850
	anhydrite		2,920
Lower Permian (sedimentary)	Sand-, silt-, claystone	below -3,000	2,700

Estimation of the minimum and maximum horizontal stresses

($\sigma_{xx} = S_{Hmax}$ and $\sigma_{yy} = S_{hmin}$)

The 3D model of the geothermal aquifer area displays fault throw characteristics (Fig. 3) that are only compatible with stress regimes that range from normal faulting (Fig. 4, case II) to strike-slip faulting (Fig. 4, case IV) including the transitional type between these two regimes (Fig. 4, case III), respectively.

Within the boundary conditions of the calculated stress polygon, the maximum and minimum allowable stress magnitudes for a normal faulting regime ($S_V > S_{Hmax} > S_{hmin}$) (case II in Fig. 4) can be calculated:

$$S_{Hmax} \leq 0.78 S_V , \quad \text{eq. (4)}$$

$$S_{hmin} \geq 0.55 S_V .$$

For a transitional stress regime between normal faulting and strike-slip faulting ($S_V = S_{Hmax} > S_{hmin}$) (case III in Fig. 4), these are:

$$S_{Hmax} = 1.00 S_V , \quad \text{eq. (5)}$$

$$S_{hmin} \geq 0.55 S_V .$$

For a strike-slip regime ($S_{Hmax} > S_V > S_{hmin}$) (case IV in Fig. 4) these are:

$$S_{Hmax} \leq 2.10 S_V , \quad \text{eq. (6)}$$

$$S_{hmin} \geq 0.79 S_V .$$

If these ratios are applied to the vertical stress magnitude of $S_V=100$ MPa acting in the reservoir, a normal faulting stress regime of case (II) (in Fig. 4) would be characterized by $S_V=S_1=100$ MPa, $S_{Hmax}=S_2=78$ MPa and $S_{hmin}=S_3=55$ MPa. A transitional stress regime of case (III) (Fig. 4) between normal faulting and strike slip faulting would be characterized by $S_V=S_1=100$ MPa, $S_{Hmax}=100$ MPa and $S_{hmin}=S_3=55$ MPa. A strike slip regime of case (IV) (Fig. 4) would be characterized by $S_V=S_2=100$ MPa, $S_{Hmax}=S_1=210$ MPa and $S_{hmin}=S_3=79$ MPa. Results from hydraulic fracturing treatments in the reservoir, that are described in detail by Legarth et al. (2005) and Reinicke et al. (2005), indicate a minimum horizontal stress of approximately 53 ± 3 MPa at a depth of 4,100 m. This in-situ stress value is inferred from measured pressures that were necessary to induce a hydraulic fracture whilst reservoir stimulation.

Compared with the results of hydraulic fracturing it can be concluded that the in-situ stress regime ranges between normal to strike slip faulting (case II and III in Fig. 4), since the stress ratio of $S_{hmin} \geq 0.55 * S_V$ is compatible with the in-situ minimum horizontal stress magnitude derived by stimulation. S_{Hmax} would be allowed to achieve a magnitude of 78 MPa (case II) to 100 MPa (case III). The compatibility of calculated and measured values of the minimum horizontal stress also shows that the reservoir rock is in frictional equilibrium. A strike slip regime with a ratio of $S_{hmin} \geq 0.79 * S_V$ does not reasonably fit to the in-situ determined minimum horizontal stress of $S_{hmin} \sim 53$ MPa.

Potential stress state along faults

It is well known that the potential fluid flow along faults is closely related to the state of stress along faults (Barton et al. 1995; Zhu and Wong 1997; Ito and Zoback 2000; Gudmundsson 2000; Zhang et al. 2002; Zhang et al. 2007), although a lot of rock properties and rock mechanical parameters have also a strong influence on the permeability of faults (Zhang et al. 2007). There are two stress state types on faults that are considered to control the hydraulic activity of faults: (1) critically stressed faults, that are close to or actually slipping, are considered as potential pathways for fluids in fractured aquifers of sedimentary and crystalline rock in Barton et al. (1995) and Ito and Zoback (2000 and the references therein); (2) extensional faults or fractures that are the main fluid-conducting pathways in e. g. Gudmundsson (2000) or Gudmundsson et al. (2002). If the in-situ stress field is known, the acting stresses along any oriented fault can be calculated thus both critically stressed and extensional faults can be discriminated by resolving the amount of shear and normal stress on any fault plane. A technique that allows the assessment of slip or dilatation potential for mapped or suspected faults in a known or inferred stress state is the slip-tendency analysis described by Morris et al. (1996), who developed this technique to estimate the reactivation potential and seismic-risk of faults. Applying this technique, we calculated the shear stress, slip-tendency and dilatation-tendency along the detected faults of the reservoir compartment in order to roughly assess the potential fluid flow along the faults. For this purpose the 3D fault model is used that describes the spatial distribution of the fault surfaces. The direction of the maximum horizontal stress $S_{Hmax} \sim 18,5^\circ \pm 3.7^\circ$ needed for this approach is

provided by borehole image log analysis of hydraulically induced fractures in the reservoir.

The slip-tendency on each fault is based on the defined stress state by stress ratios and orientations of the orthogonal stresses. The slip-tendency is displayed on a lower hemisphere equal-angle stereographic projection as shown in Figure 5. Slip is likely to occur on surfaces when the resolved shear stress τ equals or exceeds the frictional resistance of sliding. The shear stress τ and resulting slip tendency τ/σ_n for four geometrically representative fault planes is calculated in a first run under a normal faulting stress system (see case II in Figure 4). In a second run it is calculated under a stress system transitional between normal faulting and strike-slip faulting (see case III in Figure 4) and finally under a strike-slip stress system (see case IV in Figure 4) (Fig. 5). The four analysed fault planes are in the direct vicinity of the well GrSk 3/90. The fault plane geometries are representative for the regional Rotliegend fault pattern, as described consisting of NW-trending major faults (fault no. 1 and 4 in Figure 5 and Table 2) and NE- to NNE-trending minor faults (fault no. 2 and 3 in Figure 5 and Table 2).

The slip-tendency is the ratio of the maximum shear stress τ divided by the normal stress σ_n on a fault surface (Morris et al. 1996):

$$\text{Slip tendency} = \frac{\tau}{\sigma_n} . \quad \text{eq. (7)}$$

The dilatation-tendency is the relative probability for a fault to dilate under 3D stress conditions and is defined by

$$\text{Dilatation tendency} = \frac{(\sigma_1 - \sigma_n)}{(\sigma_1 - \sigma_3)} . \quad \text{eq. (8)}$$

In these equations total stresses and not effective stresses are used. In our approach, however, the pore pressure that reduces the total stresses is reconsidered in the stress ratio calculation (eq. 1). An increased pore pressure would reduce the upper and lower boundary of the stress polygon thus the slip-tendency might increase. The slip-tendency for a selected fault orientation can be divided by the maximum slip tendency for all fault orientations in the defined stress state in order to specify the selected fault as close or far from slip. This probability of slip is described by the maximum slip-tendency τ_{smax} for each fault in Table 2.

The fault plane poles in Figure 5 illustrate the results of slip- and dilatation-tendency. The red area of the lower hemisphere defines a high slip tendency

whereas the yellow to green areas have a lower slip-tendency. Effectively, fault poles that fall into the red areas have a high tendency of slip whereas fault poles that fall into yellow to green areas represent fault planes with a lower slip tendency. In Table 2 the values of slip- and dilatation-tendency are listed together with the maximum slip-tendency of each fault and in the three possible stress regimes, which are provided by the stress field calculation above.

The faults with the highest slip- and dilatation-tendencies in the normal faulting (case II in Fig. 4) and transitional (case III in Fig. 4) stress regimes, are the NNE- to NE-striking faults (fault number 2 and 3 in Fig. 5 and Table 2). This is indicated by a high maximum slip-tendency of 94.7 % - 96.8 % in a normal faulting stress regime and 99.6 to 98.0 % in a transitional stress regime. In a strike slip stress regime the NE-SW striking, SE dipping fault (fault number 2, see Table 2) shows the highest slip- and dilatation-tendency, indicated by a maximum slip-tendency of 75.6 %.

For the specification of the fault permeability related to the current stress field of all faults the faults of highest slip- and dilatation-tendency are assumed as the flow pathways. Critically stressed faults are fault planes with a high shear stress to normal stress ratio (high slip-tendency) whereas extensional faults have a low normal stress acting on the fault plane and have therefore a high dilatation-tendency. In contrast, the faults of low slip- and dilatation-tendency might be characterized by a low potential for flow. Thus the NW-SE striking faults are defined as low-flow-structures whereas the NNE- to NE striking faults are defined as high-flow-structures.

It should be stated, that additional data from borehole images, core analysis and high resolution seismic would give a deeper insight into the permeability range of the natural fracture system and some modification of the results could be the consequence. In this case study we demonstrate, however, how the in-situ reservoir stress field can be derived and interpreted although a reduced data set is available.

Fig. 5

Table 2 Dynamic characteristics of the fault pattern of the Groß Schönebeck field. The four fault planes are in the vicinity of the wells, the geometry however is characteristic for the regional fault pattern. NF - Normal faulting, TT - hybrid normal to strike slip faulting, SS - strike slip faulting, SlipTend - slip-tendency given by τ / σ_n , $\tau_{smax(\%)}$ - maximum slip-tendency for the fault plane given by the slip-tendency for a selected fault divided by the slip-tendency of all fault orientations in the current stress state, DilTend – dilatation-tendency given by $(\sigma_1 - \sigma_n) / (\sigma_1 - \sigma_3)$. In bold are the fault planes, which have the highest slip-dilatation-tendency and are therefore supposed to be hydraulically active fractures in the current stress field. Further discussion see text.

No	Fault plane	Stress Regime	SlipTend	$\tau_{smax(\%)}$	DilTend
	Dip azimuth direction/dip angle				
1	242/72	NF	0.25	71.2	0.62
2	129/57	NF	0.34	94.7	0.65
3	300/50	NF	0.34	96.8	0.57
4	255/46	NF	0.29	81.3	0.42
1	242/72	TT	0.31	89.5	0.43
2	129/57	TT	0.34	99.6	0.62
3	300/50	TT	0.34	98.0	0.57
4	255/46	TT	0.29	83.9	0.37
1	242/72	SS	0.54	77.3	0.49
2	129/57	SS	0.52	75.6	0.80
3	300/50	SS	0.40	57.9	0.82
4	255/46	SS	0.47	67.5	0.66

For the specification of the fault permeability related to the current stress field of all faults the faults of highest slip- and dilatation-tendency are assumed as the flow pathways. Critically stressed faults are fault planes with a high shear stress to normal stress ratio (high slip-tendency) whereas extensional faults have a low normal stress acting on the fault plane and have therefore a high dilatation-tendency. In contrast, the faults of low slip- and dilatation-tendency might be characterized by a low potential for flow. Thus the NW-SE striking faults are defined as low-flow-structures whereas the NNE- to NE striking faults are defined as high-flow-structures.

It should be stated, that additional data from borehole images, core analysis and high resolution seismic would give a deeper insight into the permeability range of the natural fracture system and some modification of the results could be the consequence. In this case study we demonstrate, however, how the in-situ

reservoir stress field can be derived and interpreted although a reduced data set is available.

Discussion

The fault pattern of the Rotliegend consists of two main fault populations: a major set of NW-trending faults, and a minor set of NE-trending faults. Franke et al. (1989) inferred from their work a more or less orthogonal fault system in the Rotliegend that is build up of prominent NW-SE and NE-SW striking lineaments. Baltrusch and Klarner (1993) re-processed and interpreted some seismic lines and well data and concluded a Rotliegend wrench fault system of major NW-SE faults and associated minor NE-SW striking graben structures. The interpreted fault pattern around Groß Schönebeck agrees rather with the results from Baltrusch and Klarner (1993) than with Franke et al. (1989) (Fig. 6). The difference to Baltrusch and Klarner's results (1993) is the obvious existence of NE-SW oriented major faults that intersect NW-SE faults. The NE-SW fault direction is probably not only related to minor graben structures. The question of the dominating fault direction can only be answered by interpretation of additional data and the integration of more 2D seismic sections to the existing 3D fault model could reveal additional information about the structural framework. No conclusions can be drawn about the Rotliegend kinematics as done by Baltrusch and Klarner (1993) because it is not clear from the 3D structural model whether all faults in the Rotliegend successions were generated in the same phase.

Fig. 6.

McCann (1998) infers from the petrography of Rotliegend sediments crustal segmentation and fault controlled basin formation inducing regional sedimentation patterns followed by a stable environment until the end of the Rotliegend. The 3D structural model supports the segmentation of the Rotliegend in fault blocks, but obviously some faults were active also after the Lower Permian because they crosscut the Zechstein base. Considering the results of Scheck et al. (1999), it is probable that some faults might have been generated or modified in extensional phases after Rotliegend times. According to Weinlich (1991) the Rotliegend fault system in Brandenburg is characterised by NW-SE

striking faults that were active throughout the Upper Permian (Zechstein) and formed boundaries of en-echelon arranged crustal flakes.

From this discussion it is obvious that the current stress regime cannot be inferred only from the 3D structural model since the observed fault throw may include all fault movements since Rotliegend times. The frictional failure theory additionally with the resulting minimum horizontal stress magnitude known from hydraulic fracturing is a method to limit reasonably the potential stress regimes between normal and strike slip faulting. The analysis of borehole breakouts is another common method to determine the in-situ stress field. In the well GrSk 3/90 borehole breakouts were analysed by a fracture mechanical approach (Moeck and Backers 2006). The fracture mechanical study combined with numerical modelling provides the magnitude of the maximum horizontal stress $S_{Hmax} \sim 95-100$ MPa supporting the results of the frictional failure calculation (Table 3). Borehole breakout data, however, are not always available. Hence, the combined approach of 3D structural model analysis, frictional failure theory and slip-tendency analysis might represent an alternative for deriving the current stress state at any crustal depth.

Table 3 Comparison of the stress values calculated empirically by the frictional equilibrium (after Jaeger et al. 2007), derived from fracture mechanics modelling (Moeck and Backers 2006), and from hydraulic fracturing (Legarth et al. 2005). The vertical stress S_V is 105 MPa.

<i>Empirical (frictional equilibrium)</i>		<i>Explicit (fracture mechanics)</i>	<i>Hydraulic fracturing test</i>
S_{Hmax}	S_{hmin}	S_{Hmax}	S_{hmin}
0.78-1.00 S_V	0.55 S_V	95-100 MPa	53±3 MPa
78-100 MPa	55 MPa		

The calculated stress field for the geothermal aquifer agrees with the work of Röckel and Lempp (2003) where normal to strike slip faulting stress regimes are assumed for the Lower Permian of NEGB based on several borehole breakout analyses. Lempp and Lerche (2006) investigated the stress directions in the subsalt (below Zechstein) and suprasalt (above Zechstein) and divided the North German Basin in a western, central and eastern part. Their decision tree method of stress data from boreholes implies a N-S trend of the subsalt maximum horizontal stress direction S_{Hmax} . Nearly one forth of the stress values belong to data points near a NW-SE striking fault below a salt structure. In fact, the well location at

Groß Schönebeck is in agreement with this data point definition because it is situated near a major NW-SE fault below a salt ridge.

The observed stress direction of $S_{Hmax} \sim 18,5^\circ \pm 3.7^\circ$ in the Rotliegend at Groß Schönebeck can be found in stress directions illustrated in the world stress map (Zoback 1992) and in further analysis of borehole breakouts in the NEGB (Roth et al. 1999). In fact, the understanding of the state of stress helps to describe the reservoir condition in terms of a reservoir flow simulation (Gehrke et al. 2006). The faults of high slip- and dilatation-tendency are considered as preferential flow path directions whereas the faults with a low shear stress and a high normal stress are assumed as no-flow boundary. Related to the current stress field, the NNE- to NE-trending faults define the preferential flow paths whereas NW-trending faults act as no-flow boundaries. Hydraulic tests in the new well at Groß Schönebeck will give further insight into preferential flow paths in the reservoir.

Conclusions

It is demonstrated how pre-existing data can be re-used in order to develop a 3D structural model with a modern 3D visualisation software. The 3D model describes both the morphology of the geological formations and the fault pattern that is decoupled by the Zechstein salt into a subsalt and suprasalt fault system. The Rotliegend fault system is dominated by major NW-SE and minor NE-SW trending faults. The NNE- to NE-oriented moderately dipping faults bear the highest shear stresses related to the current stress field, and as critically stressed faults they are supposed to act as hydraulically conductive structures. Various normal fault directions that are related to hinges of salt antiforms characterize the suprasalt fault pattern.

The dominating structure of the suprasalt succession is given by the Zechstein morphology of NE-SW trending salt ridges and the location of salt synforms. The Tertiary layers equalize the salt movement induced morphology of the suprasalt successions. Despite its uncertainties the 3D model remains the most detailed geological model of the Groß Schönebeck area until more or newly generated seismic data is incorporated into a new model. Since additional 2D seismic data is available for the area of northern Brandenburg, future work will focus on the integration of more 2D seismic data to extend and refine the existing geological 3D model.

The combination of fault throw analysis from a 3D structural model and the empirical approach based on the frictional failure theory and slip-tendency analysis provides a limitation of the possible in-situ stress regime in the Lower Permian of the Groß Schönebeck geothermal aquifer system. This limitation is explained by the throw of faults in the Rotliegend where no reverse faulting can be observed, indicating a stress regime between normal faulting and a transition to strike-slip faulting. The allowable minimum horizontal stress after the frictional failure theory is $S_{\text{hmin}} \geq 0.55 \cdot S_{\text{V}} = 55 \text{ MPa}$, applying a coefficient of friction $\mu = 0.85$ and a vertical stress of $S_{\text{V}} = 100 \text{ MPa}$. This result is supported by hydraulic fracturing tests that indicate a minimum horizontal stress $S_{\text{hmin}} \sim 53 \pm 3 \text{ MPa}$. The allowable stress values for S_{Hmax} range from 78 MPa (in a normal faulting regime) to 100 MPa (in a transitional stress regime between normal and strike slip faulting). Compared with the results from a geomechanical analysis of borehole breakouts the stress regimes and their magnitudes seem reasonable. The geomechanical study incorporated core tests and numerical modelling and indicates similar results for the stress values of S_{Hmax} , ranging from 95 to 100 MPa.

The slip-tendency analysis is a useful perspective to describe fault behaviour within the current stress field by resolving the shear and normal stress distribution on mapped or suspected faults. Critically stressed and extensional faults considered as hydraulically active in geothermal aquifer systems can be discriminated from any fault populations. It should be stated that the slip-tendency method is basically used to assess the slip or reactivation potential of faults in a known or inferred stress state. This should be of special interest in the development of man-made geothermal reservoirs, where pore pressure changes induced by water injection while hydraulic fracturing belongs to reservoir treatment strategies.

Acknowledgements Special thank is addressed to Agust Gudmundsson and an anonymous referee for helpful and improving comments on this article. Thank is also addressed to D. Bruhn and H. Milsch for valuable advice. We wish to thank Gaz de France-PEG for data release, specially G. Voigtländer and C. Schreyer for friendly cooperation. The 3D model is processed with earthVision[®], Dynamic Graphics Inc. (DGI) and 3Dstress, Midland Valley. This multidisciplinary project is a joint research project funded by BMWi, BMBF, BMU, MWI and MWFK.

References

- Baltrusch S, Klamer S (1993) Rotliegend-Gräben in NE-Brandenburg. *Z dt geol Ges* 144: 173-186
- Barton CA, Zoback MD, Moos D (1995) Fluid flow along potentially active faults in crystalline rock. *Geology*, 23(8), 683-686
- Bayer U, Maystrenko Y, Hoffmann N, Scheck-Wenderoth M, Meyer H (2003) 3D structural modelling and basin analysis of the Central European Basin System (CEBS) between North Sea and Poland. *Terra Nostra* 3: 1-4
- Byerlee J (1978) Friction of rocks. *Pure and Applied Geophysics* 116: 615-626
- Gast R, and Gundlach T (2006) Permian strike slip and extensional tectonics in Lower Saxony, Germany. *Int J Earth Sci* 157(1): 41-55
- Gehrke D, Moeck I, Schafmeister M-Th, Blöcher G, Zimmermann G (2006) 3D thermo-hydraulic modelling for the geothermal reservoir of Groß Schönebeck (North East German Basin). *GeoBerlin 2006*, 158th annual conference of the DGG, abstract volume: 103
- Grote R (1998) Die rezente horizontale Hauptspannung im Rotliegenden und Oberkarbon in Norddeutschland. *Erdöl Erdgas Kohle* 114(10): 478-482
- Gudmundsson A (2000) Active fault zones and groundwater flow. *Geophys Res Lett* 27(18): 2993-2996
- Gudmundsson A, Fjeldskaar I, Brenner SL (2002) Propagation pathways and fluid transport in jointed and layered rocks in geothermal fields. *J Volcanol Geotherm Res* 116, 257-278
- Franke D, Hoffman N, Kamps J (1989) Alter und struktureller Bau des Grundgebirges im Nordteil der DDR. – *Z angew Geol* 35(10/11), 289-297
- Hecht CA, Lempp C, Scheck M (2003) Geomechanical model for the post-Variscan evolution of the Permocarbiniferous-Mesozoic basins in Northeast Germany. *Tectonophysics* 373: 125-139
- Holl H-G, Moeck I, Schandlmeier H (2005) Characterization of the tectono-sedimentary evolution of a geothermal reservoir - implications for exploitation (Southern Permian Basin, NE Germany). *Proceedings, World Geothermal Congress, Antalya, Turkey*
- Ito T, Zoback M.D (2000). Fracture permeability and in situ stress to 7 km depth in the KTB scientific drillhole. *Geophys Res Lett* 27: 1045-1048
- Jaeger JC, Cook NGW, Zimmermann RW (2007) *Fundamentals of Rock Mechanics*. 4th Edition, Blackwell Publishing, Oxford, UK
- Kaiser A, Reicherter K, Hübscher C, Gajewski D (2004) Variation of the present-day stress field within the North German Basin – insights from thin shell FE modeling based on residual GPS velocities. *Tectonophysics* 397: 55-72
- Kopf M (1965) *Feldgeologie–Dichtebestimmung, Norddeutsch-Polnisches Becken, Ergebnisbericht*. VEB Geophysik Leipzig, Unpublished Report, 47 pp
- Legarth B, Huenges E, Zimmermann G (2005) Hydraulic fracturing in a sedimentary geothermal reservoir: Results and implications. *Int J Rock Mech & Mining Sci* 42: 1028-1041.
- Lempp C, Lerche I (2006) Correlation of stress directions across the North German Basin: suprasalt and subsalt differences. *Z dt Ges Geowiss* 157(2): 279-298
- McCann T (1998) Sandstone composition and provenance of the Rotliegend of the NE German Basin. *Sedimentary Geology* 116: 177-198

- Marotta AM, Bayer U, Thybo H (2000) Origin of the regional stress in the North German Basin: results from numerical modelling. *Tectonophysics* 360: 245-265
- Marotta AM, Bayer U, Thybo H, Scheck M (2002) The legacy of the NE German Basin – reactivation by compressional buckling. *Terra Nova* 12: 132-140
- Mazur S, Scheck-Wenderoth M, Krzywiec P, (2005) Different modes of the Late Cretaceous–Early Tertiary inversion in the North German and Polish basins. *Int J of Earth Sci* 95(5-6): 782-798
- Moeck I, Backers T (2006) New ways in understanding borehole breakouts and wellbore stability by fracture mechanics based numerical modelling. EAGE 68th Conference and Exhibition, 12-15 June 2006, extended abstracts volume, CD-ROM, P214, Vienna, Austria
- Moeck I, Blöcher G, Koch-Moeck M, Holl H-G (2006) 3D structural model building based on 2D seismic and well data using kriging with external drift. IAMG 11th International Congress – Quantitative Geology from Multiple Sources, E. Pirard, A. Dassargues and H.-B. Havenith (eds), Extended Abstract Volume, S14-21, Society for Mathematical Geology, 3-8 September, Liege, Belgium
- Morris A, Ferrill DA, Henderson DB (1996) Slip-tendency analysis and fault reactivation. *Geology* 24(3): 275-278
- Moos D, Zoback MD (1990) Utilization of observations of well bore failure to constrain the orientation and magnitude of crustal stresses: Application to continental, Deep Sea Drilling Project, and Ocean Drilling Program boreholes. *J of Geophy Res* 95: 9305-9325
- Peška P, Zoback MD (1995) Compressive and tensile failure of inclined well bores and determination of in situ stress and rock strength. *J of Geophy Res*, 100, B7, 12,791-12,811
- Reinicke A, Zimmermann G, Huenges E, Burkhardt H (2005) Estimation of hydraulic parameters after stimulation experiments in the geothermal reservoir Groß Schönebeck 3/90 (North-German Basin). *Int J Rock Mech & Mining Sci* 42(7-8): 1082-1087
- Röckel T, Lempp C (2003) Der Spannungszustand im Norddeutschen Becken. *ERDÖL ERDGAS KOHLE*, 119, 2, 73-80
- Scheck M, Bayer U, Lewerenz B (2003) Salt redistribution during extension and inversion inferred from 3D backstripping. *Tectonophysics* 373: 55-73
- Scheck M, Bayer U, Otto V, Lamarche J, Banka D, Pharaoh T (2002) The Elbe Fault System in North Central Europe – a basement controlled zone of crustal weakness. *Tectonophysics* 360: 281-299
- Scheck M, Barrio-Alvers L, Bayer U, Götze HJ (1999) Density structure of the Northeast German Basin: 3D Modelling along the DEKORP line BASIN96. *Phys Chem Earth (a)* 24(3): 221-230
- Scheck M, Bayer U (1999) Evolution of the Northeast German Basin – Inference from structural model and subsidence analysis. *Tectonophysics* 313: 145-169
- Weinlich M (1991) Rotliegendbruchsystem und basaler Zechstein in Brandenburg. *Z dt geol Ges* 142: 199-207
- Ziegler PA, Dezes P (2005) Crustal Evolution of Western and Central Europe. In: D. Gee and R. A. Stephenson (Es.), *Europe Lithosphere Dynamics*. *Memoirs of the Geological Society (London)*
- Ziegler PA (1990) *Geological Atlas of Western and Central Europe*, 2nd edn. Shell Int. Petroleum Mij BV and Geol Soc of London (London): 1-239

Zimmermann G, Reinicke A, Blöcher G, Milsch H, Holl HG, Moeck I, Brandt W, Saadat A, Huenges E (2007) Well path and stimulation treatments at the geothermal research well GtGrSk4/05 in Groß Schönebeck. Proceedings, 32nd Workshop on Geothermal Reservoir Engineering, Stanford, CA (USA): SGP-TR-183

Zhang X, Koutsabeloulis N, Heffer K (2007) Hydromechanical modeling of critically stressed and faulted reservoirs. AAPG Bulletin 91(1): 31-50

Zhang X, Sanderson DJ, and Barker AJ (2002) Numerical study of fluid flow of deforming fractured rocks using dual porosity permeability model. Geophys J Int 151(2): 452-468

Zhu W, Wong T-F (1997) The transition from brittle faulting to cataclastic flow in porous sandstone: permeability evolution. J Geophys Res 102: 3027-3041

Figures

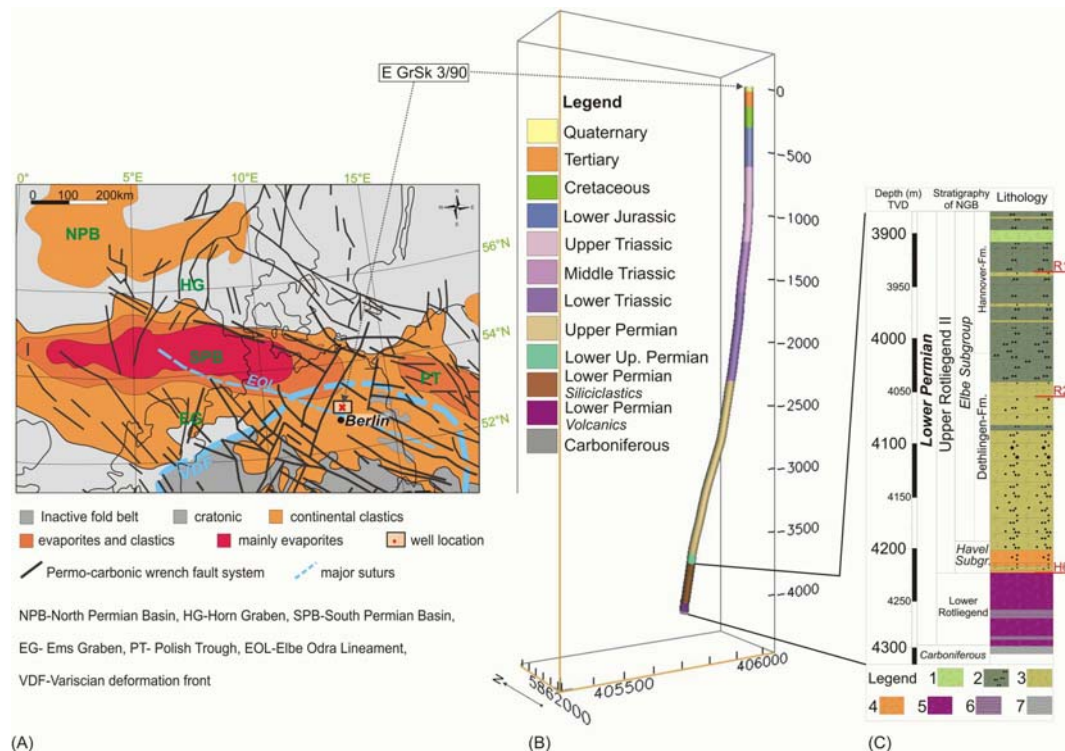


Fig. 1 Geological setting of the geothermal reservoir in the Lower Permian strata of the NEGB, in the vicinity of the Groß Schönebeck field. (A) General lithofacial structural map of the Rotliegend in North Central Europe (synthesis of Gast and Gundlach 2006; Ziegler and Dezes 2005; Ziegler 1990; Scheck et al. 2002). (B) The geothermal research well GrSk 3/90 and its geological profile. (C) The Lower Permian (Rotliegend) strata along the well. Legend: 1-claystone, 2-siltstone, 3-sandstone, 4-coarse grained sandstone, conglomerate, 5-andesitic volcanics, 6-tuffitic, marly interbeds, 7-turbiditic sediments. R1, R2, H6-seismic reflectors in the Lower Permian of the NEGB.

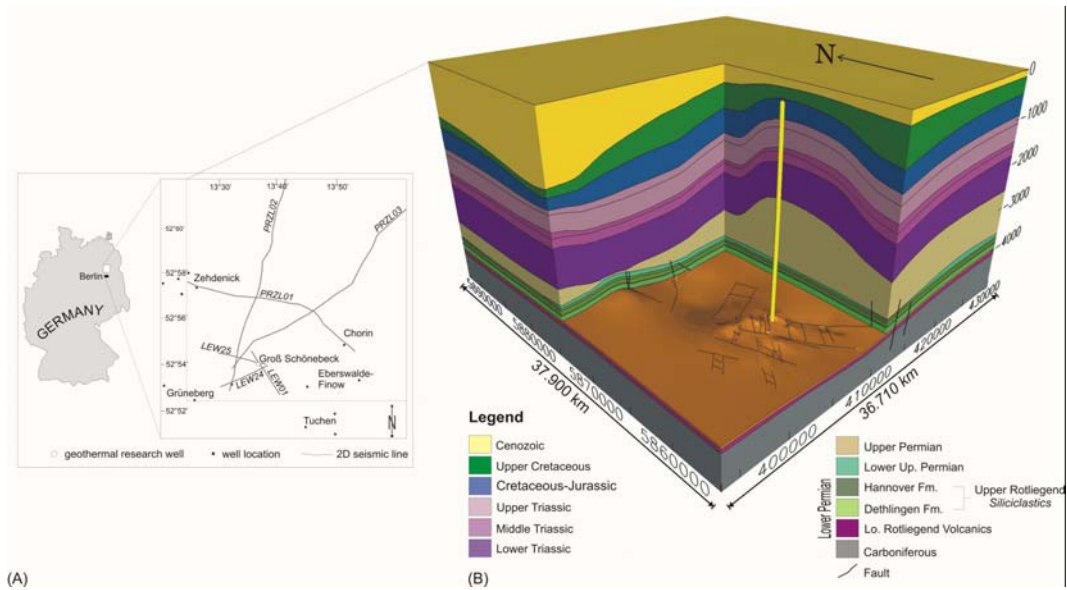


Fig. 2 (A) Localisation of the model area and distribution of the data, that consists of 15 deep wells and six 2D seismic sections. The input data were generated during the gas exploration in East Germany and are now re-used for geothermal exploration. (B) Comprehensive 3D geological model that is developed from the seismic and well data. The yellow tube represents the geothermal research well GrSk 3/90 at Groß Schönebeck. In the vicinity of the well the Lower Permian fault pattern is built up of major NW-SE and minor NE-SW striking faults.

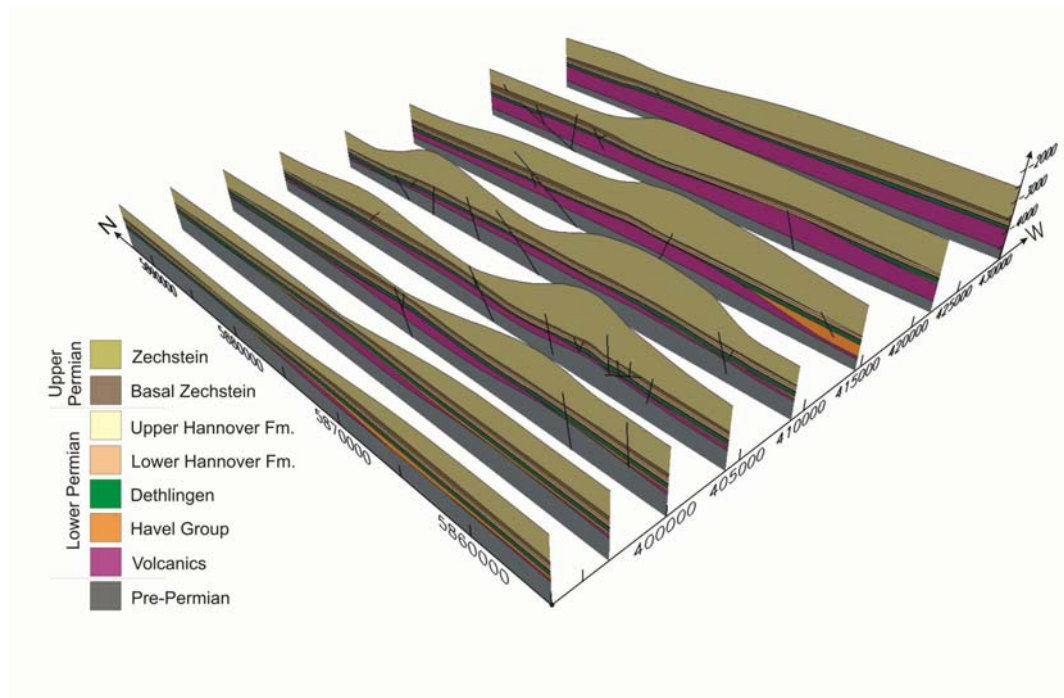


Fig. 3 Geological model of the Permian in the Groß Schönebeck area. The N-S striking vertical profiles are exerted from the 3D structural model and visualize the thickness variation and faults of the Permian successions. The fault throw indicates downward displacement of the hanging walls. Each profile is 35 km long.

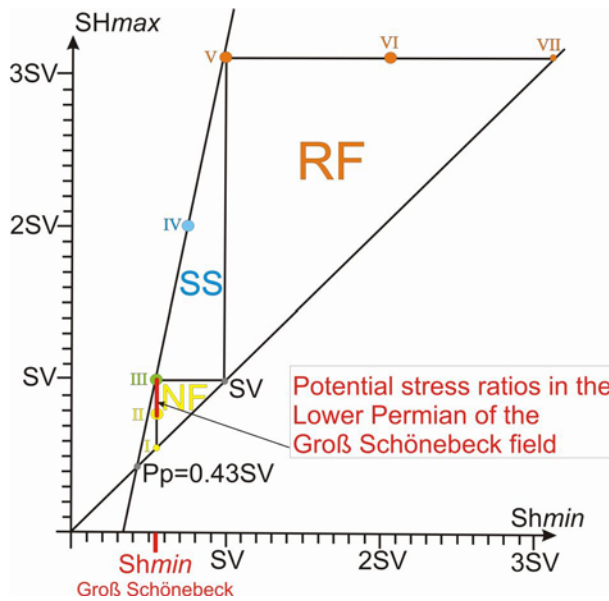


Fig. 4 Allowable horizontal stresses and stress ratios with related stress regimes in the crust based on the frictional equilibrium (after Peška and Zoback, 1995). The stress polygon is normalized to S_V and is related to the depth of the Lower Permian in the NEGB in the vicinity of the Groß Schönebeck compartment. The friction coefficient is assumed as $\mu = 0.85$. The pore pressure of 43 MPa is known from the well GrSk 3/90. NF-normal faulting, SS-strike slip, RF-reverse faulting. I to VII: cases of stress regimes defined by certain stress ratios. I-radial extension, II-normal faulting, III-transition normal-strike slip faulting (hybrid case), IV-strike slip faulting, V-transition strike slip-reverse faulting, VI-reverse faulting, VII-radial compression. Further explanation see text.

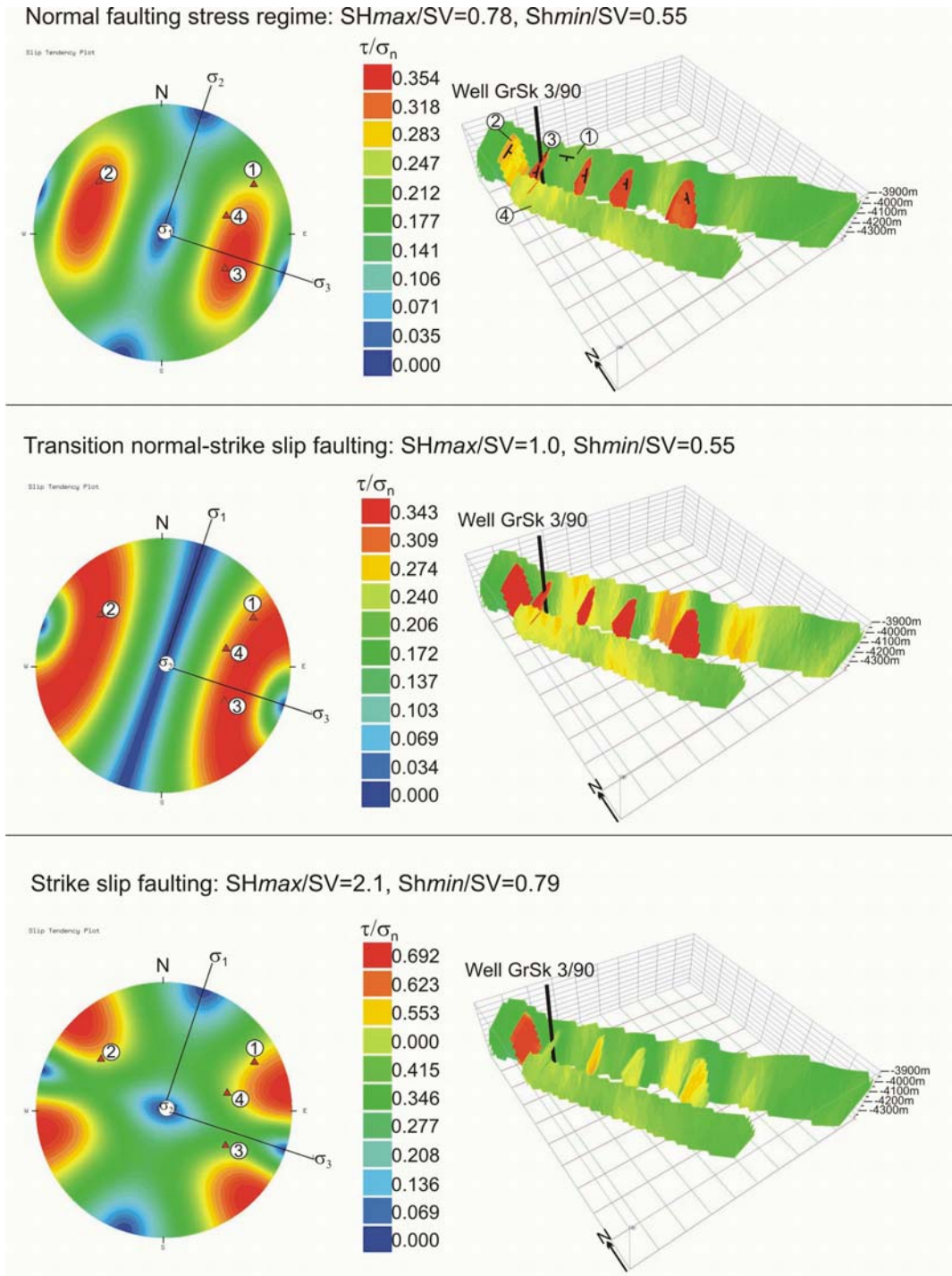


Fig. 5 Slip tendency plot for the four fault planes that surround the geothermal well GrSk 3/90. At the left the faults are displayed as poles in the lower hemisphere projection. The fault numbers correspond to the hierarchy of Table 2, where the dip direction and the dip angle of each fault are included. At the right the spatial extension of the fault system and the slip-tendency along the faults are visualized in the 3D fault model. The slip-tendency for a given fault pole is indicated on the colour scale where red indicates a relatively high slip-tendency and blue indicates a relatively low slip-tendency.

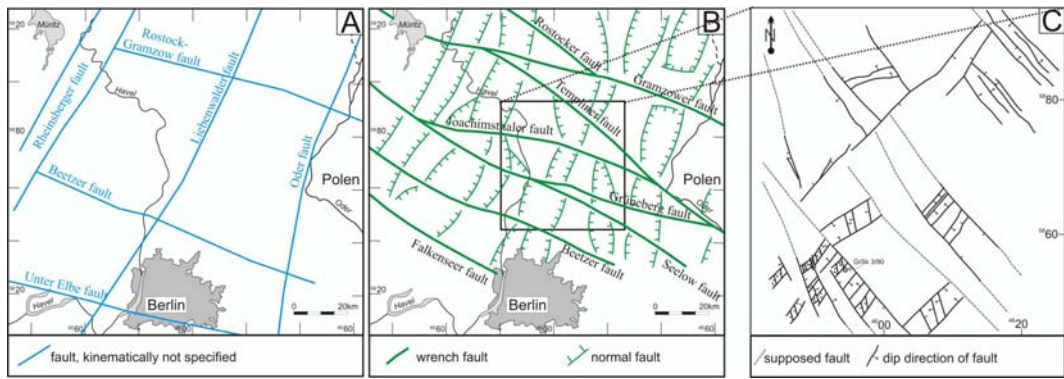


Fig. 6 Comparison of structural maps of the Rotliegend north of Berlin. (A) Tectonic map of NE Germany according to Franke et al. (1989), (B) structural map according Baltrusch and Klarner (1993), (C) new structural map for the vicinity of geothermal investigation site Groß Schönebeck.